The *Precessions* Process for Efficient Production of Aspheric Optics for Large Telescopes and Their Instrumentation

D.D. Walker[a,b], A.T.H. Beaucamp[b], R.G. Bingham[a], D. Brooks[a], R. Freeman[b], S.W. Kim[c], A. King[a], G. McCavana[b], R. Morton[b], D. Riley[b], J. Simms[b]

[a]Optical Science Laboratory, Dept Physics and Astronomy
University College, Gower St, London WC1E 6BT

[b] Zeeko Ltd, at ACC Systems Ltd, 6 Vulcan Way, Vulcan Court,
Hermitage Industrial Estate, Coalville, Leicestershire, LE67 3FW

[c] Center for Space Astrophysics, Dept. of Astronomy and Space Science,
Yonsei University, 134 Shinchon-dong, Seodaemun-gu
Seoul 120-749, Korea (South)

ABSTRACT

We summarise the reasons why aspheric surfaces, including non-rotationally-symmetric surfaces, are increasingly important to ground and space-based astronomical instruments, yet challenging to produce. We mainly consider the generic problem of producing aspheres, and then lightweight segments for the primary mirror of an Extremely Large Telescope. We remark on the tension between manufacturability of spherical segments, and performance with aspheric segments. This provides the context for our presentation of the novel *Precessions* process for rapid polishing and form-correction of aspheric surfaces. We outline why this is a significant step beyond previous methods to automate aspheric production, and how it has resulted in a generalized, scaleable technology that does not require high capital-value tooling customized to particular types of optical form. We summarise implementation in the first two automated CNC machines of 200mm capacity, followed by the first 600mm machine, and the current status of the process-development programme. We review quantitative results of polishing trials, including materials relevant to large and instrumentation optics. Finally, we comment on the potential of the technology for space optics and for removing quilting in honeycomb substrates.

1. Introduction

This paper provides a technical progress-report on the development of the *Precessions* polishing process. The process is a novel small-tool polishing method under development for producing aspheric forms and correcting spherical forms. *Precessions* polishing is being developed by Zeeko Ltd in collaboration with the Optical Science Laboratory at University College London and Loh Optikmaschinen. Three *Precessions* CNC polishing machines have been built – the original IRP200 which has been used for process development, the first of the 200mm capacity A_{II} Loh/Zeeko machines, and the Zeeko IRP600 now under commissioning at UCL. A project to build a 1m capacity machine is scheduled to commence in the last quarter of 2002. Indeed, a key feature of the *Precessions* technology is that it is directly scalable to larger sizes using the same machine architecture, (scaled) tooling and the same software.

2. Astronomical Applications of Advanced Polishing Technology

2.1 ELT primary segments

Current 30-100metre telescope projects universally adopt segmented mirror designs, but there are two schools of thought regarding the optical design. The first, exemplified by ESO's 100 metre Overwhelmingly Large Telescope ('OWL')[1], is that a primary comprising identical spherical hexagonal segments will considerably reduce the manufacturing cost, risk and time, and reduce operational problems (principally in managing aluminising cycles), compared with an aspheric primary. In particular, spherical segments can be multiply-produced on a large stiff tool by traditional lapping techniques.

Specialized Optical Developments in Astronomy, Eli Atad-Ettedgui, Sandro D'Odorico,
Editors, Proceedings of SPIE Vol. 4842 (2003) © 2003 SPIE · 0277-786X/2003/$15.00

However, warping is expected on cutting the segments to the hexagonal shape due to relaxation of stresses within the material. The penalty is that a complex and massive spherical aberration compensator is required near the nominal focus of the primary. In the case of the OWL, a recent (but still evolving) design posted on the ESO web site comprises a 33.5m diameter segmented flat M2, two 8.2m diameter active mirrors (M3,M4), a 4.3m passive M5, and a 2.5m tip/tilt M6. Significant aspheric profiles are unavoidable in the corrector optics.

The other approach is to follow the Keck project by using an elegantly simple two-mirror system, with the penalty that the primary segments are then off-axis aspheric sections. However, the solution is potentially advantageous in terms of stray-light and infrared emissivity; important for key science drivers such as extra-solar planets. This approach is being pursued by CELT [2], GSMT [3] and Euro50 [4]. The secondary is then a significant aspheric; either a convex hyperboloid (CELT, GSMT), or a Gregorian concave ellipsoid (Euro50). The Gregorian approach has the advantage of providing for an independent test of secondary form in the telescope, permitting decoupling of the adaptive correction at the secondary from active correction of the primary. The principal penalty of the aspheric primary is the challenge of producing the different aspheric segments. The need for interchange of multiple spare segments for re-aluminising, also requires careful consideration.

In the case of Euro50, the vertex radius of curvature of the whole primary mirror assembly is 85 metres. In a study on behalf of the Euro50 project [5], we have examined some of the trade-offs in the manufacture of the primary segments, which are basically torroidal. For a segment size of ~2m across the flats, and in the case of a corner segment, the mirror surface is more than +/- 300 microns from a mean sphere. The Euro50 specification for the segment polishing (part of an error budget) is <36nm peak-to-valley for form, and <18nm peak-to-valley ripple.

The *Precessions* polishing process described in this paper, with further development, is a candidate for both the rectification of OWL spherical segments after cutting, and for polishing and form-correction of aspheric segments such as required for Euro50. In the latter case it is assumed that the segments would have been pre-cut to the hexagonal shape and precision diamond-generated to the off-axis aspheric profile, as we have previously described [5].

2.2. Ground and Space Based Optical Systems

Ground-based astronomical instruments frequently use aspherics of some shape or form. These may, for example, comprise off-axis paraboloid collimators, or corrector elements in cameras. Off-axis systems can eliminate central obstructions, improving throughput. Procurement times for significant sized aspherics for large-telescope instrumentation can run from six to eighteen months or more. Automated methods such as *Precession* polishing could dramatically improve this situation. Furthermore the deterministic nature of the process should enable more ambitious surfaces to be produced regularly. This should catalyse designers to be more ambitious in adopting highly-corrected solutions, which would be considered too risky today.

Space optical systems demand compact and low-mass optical systems for imaging and re-imaging. Classic 3-mirror anastigmat designs are commonly used. Indeed, such designs were considered for the NGST project, as described by Hadaway et.al.[6]. In certain cases, these designs can demand extreme forms, and may also be constructed as off-axis segments avoiding a central obstruction. *Precessions* polishing is a strong candidate for polishing such surfaces, particularly when the full 3-D form control algorithms have been developed.

3. The *Precessions* Process

The principal challenge of polishing aspherics is the mis-match between tool and work-piece, as the tool traverses the asphere's varying local curvature. This tends to drive the classical optician to very small tools for severe aspherics, resulting in tool edge-effects, surface defects and low removal-rates. The *Precessions* process uses passive compliant tooling which is effectively 'universal', and whose absolute motion and orientation in space is orchestrated by an active 7-axis CNC system. Compared with active tools such as the Steward stressed lap[7,8], we have adopted very simple tooling, but at the expense of increased machine complexity. However, the end result is a highly effective and versatile system. As we have described [9,10,11,12], the tooling is a rotating, inflated spherical membrane tool (the 'bonnet'), which naturally moulds itself to the local aspheric surface. The bonnet is covered with a standard detachable polishing surface such as polyurethane. Inflating the bonnet increases polishing pressure. Advancing the bonnet towards the work-piece compresses

the membrane and dilates the contact-area ('polishing spot'), which itself is effectively 'edgeless'. The form of the removal-profile over the polishing spot is called the tool's 'influence function'. The machine can orientate the tool's rotation-axis to be pole-down, or precesss the axis around the local normal to the work-piece surface.

The machine must place the polishing spot at the correct position with respect to the work-piece surface to some 10 microns (IRP200), in order to polish the correct area, and to give the calculated compression of the bonnet and achieve stable influence functions. The machine also orientates the bonnet with respect to the local surface-normal, allowing both for the surface-slope and the precession angles. This is accomplished using CNC machine tool technology as commonly applied to diamond turning and grinding machines. This may be contrasted to the more traditional polishing machines, where the tool effectively floats on the surface of the part.

The Tool-Head rotates the tool at up to a nominal 1500 rpm ('H' axis), and a load cell measures contact force. The membrane is pressurized from an external air supply. Different radii membranes can be interchanged to give different ranges of contact spot diameter. The work-piece can also be rotated for producing axially-symmetric forms. The main mechanical subsystems are mounted off a cast polyquartzite base which gives a very stable platform. The CNC uses a Fanuc 16i system, housed in an electronics enclosure.

4. Status of process development

4.1 Form-preserving polishing

We have reported elsewhere[10] a summary of extensive polishing trials removing a constant depth of material (onion-skin polishing') at high stock removal rates. The bonnet was covered with cerium-oxide impregnated polyurethane, and the process used a continuous re-circulating flow of temperature-controlled cerium oxide slurry.

The principle application of form-preserving polishing is to remove surface and sub-surface damage on a part from a precision grinding machine. This may result in an optical surface ready to use, or may require further steps of form correction using the *Precessions* optimisation technique see (Sect. 4.2 below).

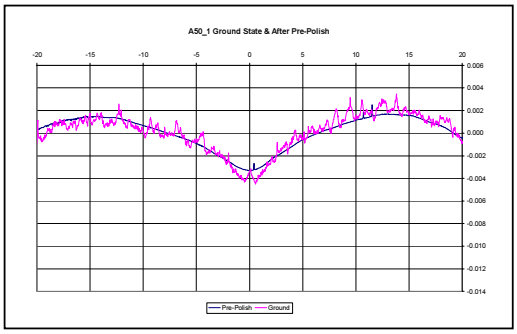

Figure 1 form-preserving polishing on aspheric

Two form-preserving methods have been used [9] i) rastering with a precessing tool on a stationary work-piece, and ii) using a pole-down tool which makes many diametric passes over a rotating work-piece.

The process has been optimised to maximise stock removal rate. Very high uniformities of removal have been achieved when removing several microns of stock. One example [9] – an aspheric lens – is repeated here as Figure 1. A 40mm zone of a 60mm lens was polished (thereby maintaining an unpolished land to define absolute removal). The asphericity in the polished zone was 125 microns relative to the sphere osculating about the vertex. 7.5 microns of stock was removed, with a uniformity of 96%.

The maintenance of such a high uniformity of removal on a surface of small diameter yet significant aspheric departure, demonstrates the ability of the membrane tool to maintain uniform polishing conditions over varying surface curvature.

4.2. Form Control

4.2.1 Method

Numerical optimisation using the *Precessions* code running on an off-line PC has already been described [10]. A family of experimental influence functions of different widths ('spot sizes') is imported, plus target and measured profiles of the work-piece surface. The optimiser defines tool-paths to be concentric rings, with variable ring-spacing, spot-size and dwell-time. The optimiser maximises a merit function derived from a weighted combination of height and slope errors, and process-time. The output is transformed into a fine spiral tool-path for execution by the machine.

The optimiser correctly handles the difficult problem of tool-overlap across centre (which otherwise tends to create a central hole), by adding the respective removal contributions. However, the resulting dwell times near centre become extremely short. This can be mitigated by moderating tool-rotation speed. As reported previously [9], removal as a function of tool speed has been shown to be almost perfectly linear over a decade of speed.

4.2.2 Results

The example of figuring a Schmidt plate on the IRP200, removing about 2 microns at the edge was described be Walker et.al [10], and achieved about 80% convergence (i.e. 20% error) in a single pass with high stock removal rate. The bonnet was covered with cerium-oxide impregnated polyurethane, and was used with a continuous flow of cerium oxide slurry.

There have been several challenges in continuing to iterate the process to improve form further. These have resulted primarily from the very short dwell times that the *Precessions* optimiser requires. There are three main reasons for this:

1. With spiral polishing, removing even a constant layer requires dwell-times that are proportional to radial distance from the centre of the work-piece, and these dwells become small near centre. This is an inherent property of the circular geometry of the process.
2. In the central zone, as soon as the polishing spot overlaps centre, the centre is being worked continuously.
3. In fine form-control, regions of the surface will require minimal removal.

Slowing the tool rotation-speed as mentioned above does not provide sufficiently fine control. For this reason, the overall removal-rate has been reduced for fine form-control, by using a combination of more dilute cerium oxide slurry, and by a move from polyurethane to Multitex on the tool-surface.

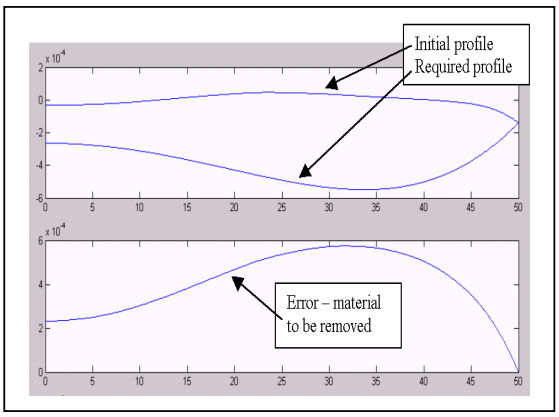

Figure 2 Required profile and measured profile on 100mm diameter part, resulting in 0.6 microns p-to-v of material to be removed

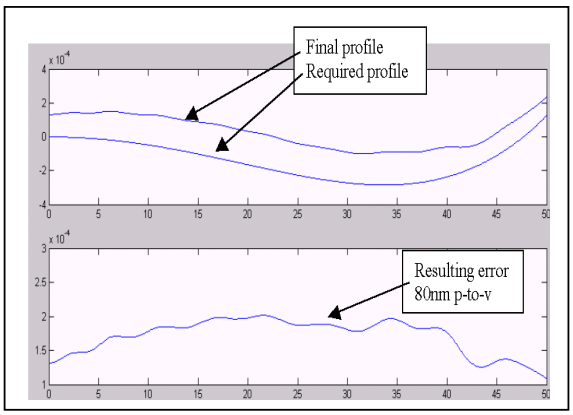

Figure 3 First result of iterative form control on 100mm diameter part: result after three polishing runs with fixed spot-size and zone-spacing

Figure 2 and 3 show the specification and results of the first iterative polishing run conducted with the *Precessions* polishing process, shortly before submission of this paper. The original surface showed some non-axially-symmetric form errors, and no attempt was made in this run to correct these (although the *Precessions* code can handle simple folding errors). Therefore, both the initial and final forms were circumferentially averaged. The machine used was the new IRP600, still under commissioning at UCL. The work-piece was a nominally flat part 100mm diameter, with a starting form-error of about 0.1 microns as measured with a Wyko 6000 interferometer. The objective was to achieve form-control by generating a mildly aspheric Schmidt-like form, requiring some 0.6 microns of material to be removed.

Normally, the *Precessions* optimiser and subsequent tool-path generator would continuously vary the spot-size, dwell-time, zone-spacing and tool-speed. However, this first run was executed using a single influence function (constant spot-size), and fixed zone-spacing, in order to develop the process systematically and simplify diagnostic analysis of the result.

For the same reason, the tool rotation speed was kept at a constant 200rpm. After three polishing runs (with Wyko 6000 interferometry between), the final profile was within 80nm peak-to-valley of the target, and the ripple within approximately 35nm peak-to-valley.

An analysis of the control files and the results indicate that a limiting factor in both form-control and ripple still tended to be the extremely short dwell times (few seconds or less) for some of the radial zones in the polishing runs. Various strategies are available to mitigate against this, including further modification to the slurry and tool-surface to reduce overall removal rate, further reduction in tool rotation-speed, adjustment of bonnet-pressure, reduction in spot-size, and an increase in the turntable speed. Freeing-up the tool-size variable in the optimisation is also expected to reduce ripple. All these will be investigated.

5. Edge-control

Control of segment-edges for an extremely large telescope is challenging. A small edge roll-off can encompass a significant area of the telescope pupil and lead to degradation of stray light performance.

Various strategies may be attempted to achieve good edges, for example:

i. The use of waister pieces i.e. sacrificial pieces of the segment material temporarily cemented around the edges prior to commencement of optical work. These are detached at the end, with the risk that cementing stresses may be released, distorting the segment.
ii. Manufacture of segments over-size, followed by edging down. This can result in re-distribution of internal material stresses, again leading to distortion.
iii. Optimisation of the intrinsic polishing process to control the edges actively.

Our favoured approach is iii above, with i reserved as a fall-back. In order to establish the extent of the problem in controlling edges with the *Precessions* process, we have conducted a preliminary experiment on the IRP600 at UCL, without taking any specific precautions to compensate for edge roll-off in the optimisation.

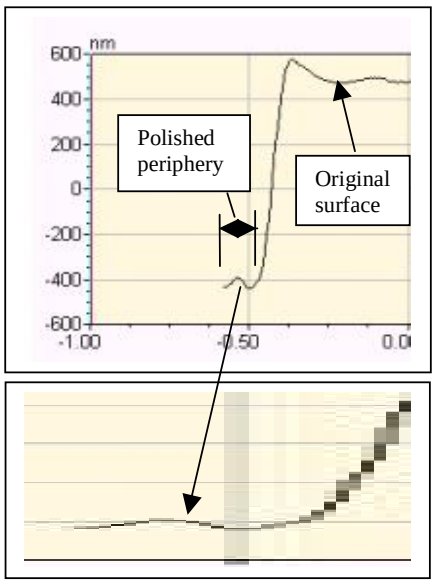

Figure 4 Polishing a peripheral zone to investigate edge-effects

The experiment involved polishing a ~15mm wide peripheral zone on the edge of the 100mm aspheric diameter work-piece resulting from the experiment shown in Figure 3 above. The tool spot-size was 9.8mm full-size and 5.8mm FWHM. The *Precessions* optimiser code was configured to remove a constant depth of material from the periphery. It was constrained to place the outermost ring of polishing so that the centre of the polishing-spot was exactly on the periphery of the glass.

1 micron of material was removed from the periphery in the polishing run, as shown using a Wyko 6000 interferometer. The initial OPD was subtracted from the final OPD, giving the difference profiles of Figure 4. The lower plot is simply a section of the upper one that has been horizontally stretched. Very little edge roll-off was observed, although the optimisation resulted in a small amount of ripple at the <50nm peak-to-valley level.

In the future, we propose to develop the optimiser code specifically to reduce ripple further (especially near the edge). As already mentioned in the context of Figure 3 above, it is believed that freeing the tool spot-size and zone-spacing variables will assist in this. The edge-test also placed all the weight in the optimisation on surface-height, and a small element of slope weighting may well improve results in the future.

6 Scaling to ELT segments

An advantage of the *Precessions* process is that it is inherently scalable. Consider the case of a work-piece of given aspheric 'difficulty'. A simple example is a parabola of specified focal ratio. Now consider the following:

1. Work-piece diameter is doubled (maintaining f/ratio).
2. Polishing bonnet radius of curvature is doubled (i.e. the physical size of the tooling is doubled).
3. Axial motion of bonnet into work-piece surface is doubled, with respect to the point of first contact.
4. Surface speed on work-piece is maintained constant by halving the tool rotation-speed.

Overall, 1-3 above change the linear scale of the experiment by the same factor in X, Y and Z. The effect is to increase both the area of the work-piece, and the area of the polishing spot, each by a factor of 4. Moreover, the match of the enlarged spot-size to the local aspheric form remains constant. By maintaining surface speed and increasing spot-size, the volumetric removal rate is increased by a factor 4, which compensates for the increased area to be polished. To first approximation, process time is therefore *independent of work-piece diameter*, for the same 'difficulty' of asphere. In practice, there is definitely scope to increase surface speed and reduce process time.

Given the high linearity observed in the process [9], and extensive measurements of volumetric removal rates on the IRP200, we have performed scaling estimates for polishing segments 2.3m across the flats [5]. To summarise, we considered the following scenario:

Polishing bonnets	400 and 800 mm R of C	Tool pressure	1 Bar
Tool motion	Precessing about local surface normal	Average spot size	180 mm full-spot (~ 90mm nominal FWHM)
Tool speed	0 to 1000 rpm	Maximum spot size	240 mm full spot (~120mm nominal FWHM)
		Polishing medium	Cerium oxide on polyurethane

Based on measured influence functions from the IRP200, we predict the scaled volumetric removal rates on BK7 to be 70 and 120 mm^3/minute. To remove 10 microns from a segment would then require approximately 3 hours of polishing. Off-axis segments would be polished by rastering the surface (rastering has already been demonstrated on the IRP200 machines for form-preserving polishing, as described above). Note that rastering has no circular symmetry and overcomes many of the limitations of spiral polishing.

7 ELT primary mirror segments: texture and ripple formed in the polishing process

7.1 Formation of texture and ripple

Texture is the microscopic topography of the surface, produced by the interactions of the population of individual slurry particles with the material being polished. Previous polishing trials on a *Precessions* polishing rig at UCL, supported by metrology on a Wyko RST500 surface texture interferometer, have demonstrated superb texture results[10]. In particular, Ra (roughness average) values down to 0.5nm have been achieved on BK7 glass, 1nm on nickel-coated aluminium (used for metal mirrors), 1nm on Stavax stainless steel (used for moulds), and 5nm on a Graphite-fibre / RS-3 cyanate-ester resin honeycomb (used for light-weight mirrors).

As regards ripple, there are two principle sources in *Precessions* polishing: i) tool spot-size and ii) zone-spacing. In relation to the former, the optimiser may not perfectly converge, and can leave residuals, typically on a scale-length of the spot-size. The recent result in Figure 3 above shows such an effect, after a run with fixed spot-size and fixed zone-spacing. Even this simple demonstration achieved peak-to-valley ripple within a factor of two of the Euro50 specification. Residuals can be reduced further by freeing the spot-size and zone-spacing variables in the optimisation.

In a raster or spiral, the tool paths overlap substantially. However, this still leaves its own characteristic ripple at some level, at the spatial frequency of the zone-spacing. The absolute peak-to-valley depth R of the surface features tends to be deterministic, and depends on:

* FWHM of Influence function
* Step-size between adjacent tool-paths
* Depth of material removed

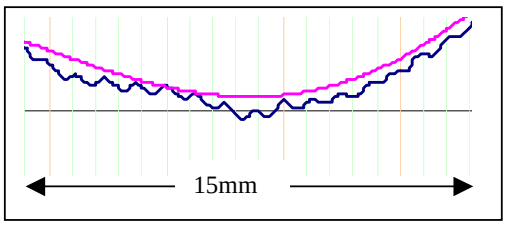

Figure 5 Example of measured ripple (50nm p-to-v), due to a coarse step-size between tool-paths

Figure 5 shows an experimental example of the surface features created with a step-size between tool-passes of 1.25mm, course for the spot-size (~7mm full-width). The figure is a magnified part of the Schmidt plate result previously reported[10]. The spot-size was variable across the work-piece, having been optimised using the *Precessions* code. The resulting amplitude of the features was approximately 50nm p-to-v. With appropriate choice of spot-size and step-size between tool-passes, the effect can be reduced to arbitrarily small amplitudes.

The formation of ripple due to the finite effect step-size has been numerically simulated, taking as input:

- an influence function measured experimentally (9.5mm full-width)
- a specified step-size between polishing traverses (0.25mm and 0.1mm)
- the dwell-time per traverse needed to give either 8.8 or 22 microns depth of removal

An example result is shown below (Figure 6). The predicted ripple is:

- 11 nm peak-to-valley for 8.7 microns depth of removal and 0.25mm step-size
- 13 nm peak-to-valley for 22 microns depth of removal and 0.1mm step-size

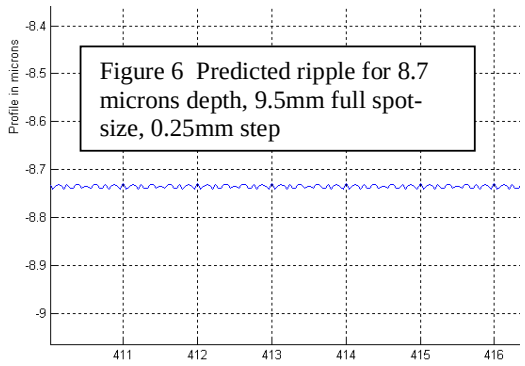

Figure 6 Predicted ripple for 8.7 microns depth, 9.5mm full spot-size, 0.25mm step

Note that scaling the process to larger spot-sizes (e.g. for larger work-pieces) preserves the *same* depth of ripple for the *same* depth of polishing. Therefore, the critical parameter is the ratio of spot-size to step-size between tool-traverses.

From the above results, spot-size to step-size ratios of between ~ 40:1 and ~ 100:1 are appropriate for polishing depths of ~9 microns and ~ 22 microns respectively.

For a 180mm spot-size on a nominal 2 metre segment, approximately 2 to 5 mm step-size between tool-passes would be required to give a nominal 12nm p-to-v ripple. In practice, a finishing pass would be expected to clean the surface further.

7.2 Stray Light from Surface Roughness or Ripple

In this section, attention is drawn to the total fraction of incident light that may be scattered from a mirror and how it may be specified and computed from surface metrology.

7.2.1 The general expression for light loss due to scattering

There are known expressions relating surface roughness and other figuring errors to scattering. However, the two basic expressions are not normally used in a single study and it is relevant to bring them together here for comparison. The root-mean-square (rms) wavefront aberration in terms of wavelengths is denoted by σ. For small aberrations, the fractional loss L of intensity in the central peak of an image that is close to the diffraction limit is simply related to the Strehl ratio [13].

$L = 1 - \exp(-(2\pi\sigma)^2) \approx 4\pi^2\sigma^2$ (i)

As pointed out by Born and Wolf [13], the formula is derived for low-order (smooth) aberrations. In contrast, the Total Integrated Scattering *S*, at normal incidence for random roughness is given by

$S = 1 - \exp(-(4\pi\delta)^2) \approx 16\pi^2\delta^2$ (ii)

where δ is the rms surface roughness as deviation from a mean plane. (See e.g. Bennett Mattsson [14])

Expression (i) applies to an optical wavefront generating an image that is close to the diffraction limit of resolution. Expression (ii) in the form shown applies to any beam of light in reflectance at normal incidence. However, in case (ii), rms wavefront errors at normal incidence are equal to 2δ. We therefore have $\delta = \sigma/2$

The two expressions are similar, despite the difference in their practical applications.

7.2.2 An example of ripple

One type of surface error capable of analysis is a linear sinusoidal ripple. An amplitude 11nm peak-to-valley on a mirror surface, with a spatial frequency of one cycle per 4.7mm has been investigated. The ripple acts as a diffraction grating, a star primarily giving rise to subsidiary peaks that are star-like (monochromatically) at orders +/- 1. This has been explored for a wavelength of 1 micron. From the above formulae, the scattered intensity is proportional to the inverse square of the wavelength. This applies to all the examples discussed below.

(1) Linear, parallel ripples, phased

The first-order (satellite) peaks for the ripple function described are +/-0.012 degrees (44 arc seconds) from the central zero-order peak at one-micron wavelength. For a range of wavelengths, the satellite peaks are dispersed in the normal way along a radius.

To find the central loss and the intensity of the satellite peaks, the Strehl formula may readily be evaluated using the theoretical rms wavefront height of the sinusoid. That is equal to 7.8nm for a peak-to-valley wavefront height of 22nm, giving a loss of central intensity equal to 0.24 per cent. A numerical rms calculation gives an identical result (when sampling is adequate). Fourier diffraction shows that this fraction of the intensity is predominantly directed into the two first-order peaks, which therefore each have intensity equal to 0.12 per cent of the central peak. A Fourier diffraction calculation of intensity gives essentially the same result in terms of central intensity as the Strehl formula. This is because the Strehl formula is valid for aberrations of fractions of a wavelength.

The central peak and the first-order peaks for the whole mirror array are the result of adding contributions from all the segments. In the case of the central peak, all the segments can add in phase despite the sinusoidal ripple, and the angular profile of the central peak is unchanged. In the case of the first-order peaks, the same result would apply if the ripple profile were aligned from segment to segment to much less than the period of 4.7mm, which could conceivably be achieved. In that case, the first-order peaks also have the diffraction-limited profile of the whole 50m aperture, ~0.005 arc second FWHM at 1.0 microns. They are dispersed with wavelength.

(2) Linear, parallel ripples, unphased

If the sinusoidal ripple is randomised in spatial phase between segments, the central peak is unaffected, and retains the diffraction-limited profile of the whole 50 m aperture. However, a different form of addition applies to the first-order diffraction peaks. In the first-order peaks, the partial wavefronts from the separate segments are incoherent if the ripple has no spatial alignment. The image envelope corresponds to the approximately circular diffraction limit from a single segment. (At a wavelength 1.0 micron, the FWHM of this single- segment image is 0.13 arc seconds and these diffraction peaks are 44 arc seconds from the axis.) The average surface brightness in these enlarged satellite images is about 2×10^{-6} as compared to the central image. Monochromatically, speckles are formed.

(3) Circular ripples

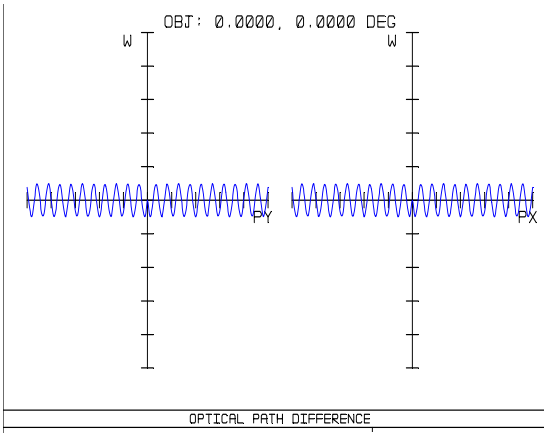

Figure 7 Cross-section of wavefront in reflection from circular ripples of surface height 11 nm peak-to-valley

If the ripples are circular and centred on a segment, the central image is again unaffected but there are now no separate first-order peaks. Instead, the main image is surrounded by a faint halo. The total diffracted intensity in this case is still 0.24 per cent of the central image at 1.0 microns wavelength, but it is spread over an annulus at 88 arc-seconds diameter.

The diffraction from the whole mirror area is not numerically computable, but the effect is qualitatively illustrated, and then estimates are made for the related diffraction effect in the real telescope. The example computed is a segment of 100 mm diameter with the same ripples. In order to increase the diffraction effect for illustration, the wavelength is reduced to 110nm, so that the p-v ripple on the wavefront is 0.2 wavelengths. Figure 7 shows cross-sections across the mirror in two planes, intersecting the circular ripples. Figures 8,9 show point-spread functions of the perfect mirror and the mirror with ripple respectively.

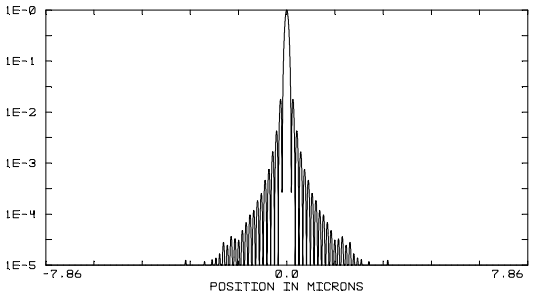

Figure 8 The point spread function from a perfect mirror of 100 mm diameter at 100 mm focal length (log scale)

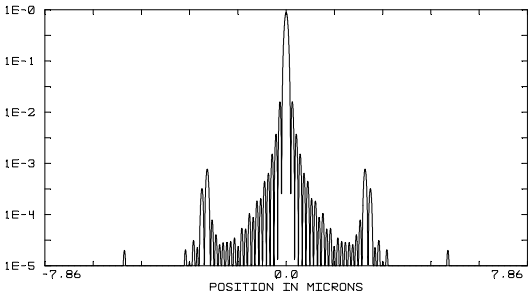

Figure 9 The point spread function of a circularly rippled 100mm mirror at 110 nm wavelength, projected to 100 mm focal length (log scale)

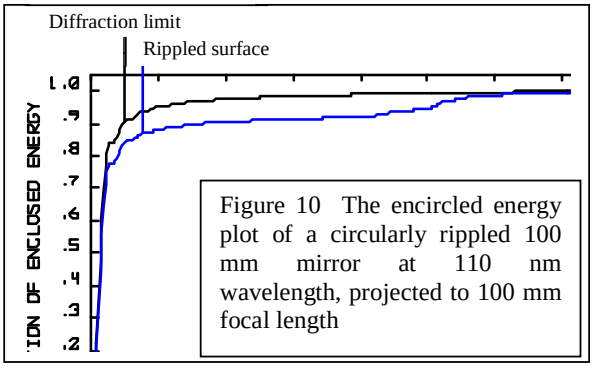

Figure 10 The encircled energy plot of a circularly rippled 100 mm mirror at 110 nm wavelength, projected to 100 mm focal length

Figure 10 shows how circular grooves redistribute the light in a partly annular form out to the first-order diffraction angle. The resolution of the central patch is unaffected. If examined with very fine sampling (monochromatic), the annulus of diffracted light would be found to enhance Airy diffraction rings, being analogous to speckles that appear in all related diffraction problems.

Owing to the relatively small number of grooves, the Strehl ratio and central intensity for the example have to be recomputed rather than being extrapolated from the previous examples.

The loss indicated by the Strehl formula is 13 per cent and by diffraction methods (preferred) is 11 per cent, in this specific illustration for a 100mm mirror. The diagrams above show that 7 to 8 per cent of the total intensity (i.e. most of the central loss) appears in the annular ring.

Semi-empirical scaling laws have been used to predict the comparable effect for the practical segments. A diffraction ring or bright annulus due to the ripples is expected at a radius of approximately 44 arc seconds at 1 micron wavelength. The ratio of apparent surface brightness of central peak to the annulus in this monochromatic case is of the order of 10^6 for a single 2m segment, and of the order of $5x10^8$ for a diffraction-limited, assembled 50m array. This value for the array makes an assumption of incoherence for the ripples in the separate segments. The integrated scattered light, mainly lying in the annulus, is still ~0.24 per cent. The annulus is radially diffused by dispersion in a broadband case. This ring would need to be compared with other extended illumination that is present due to seeing, adaptive optics and other optical components.

Overall, straight phased ripples produce two distinctive satellite images each at 0.12 per cent of the central intensity for the wavelength and other conditions stated. Straight unphased ripples produce similar ghost images, but the ghost images are relatively diffused. Circular grooves (centred separately on each segment) produce the same proportion of stray light, but distributed over a large annulus. A provisional solution in the presence of parallel ripples is to align them (either phased or unphased) so that the two satellite images appear superimposed on two opposite diffraction spikes of the whole 50 m telescope. By adjusting the ripple-spacing, the spatial extent of the light can be controlled.

8. Simulation of *Precessions* polishing for a space optical system

We have recently obtained from industry three designs for 3-mirror off-axis anastigmat systems, proposed for a future astronomy space mission. Due to reasons of commercial confidentiality, we have been told that details of the exact function and mission are currently unavailable. Nevertheless, the designs have provided an invaluable case-study into the potential for *Precessions* polishing. Of the nine surfaces in the three designs, we have selected the most difficult. The surface is an off-axis segment of a figure of revolution (see Figure 11). The parent was described to us as:

Radius of curvature	486mm
Conic constant	0.19
Diameter of parent	608mm
Off-axis mirror segment size	280 by 180mm
Off-axis distance of mirror centre	180mm
Departure from best sphere	443 microns

Manufacturing the parent and cutting a section is not an option, as the parent was described to us as "f/0.4".

Now the *Precessions* optimiser code in its current form can not handle the off-axis segment directly. Nevertheless, we considered that optimising for a 2-D section through the surface would give invaluable insight as to whether the tooling could inherently handle the aspheric departure.

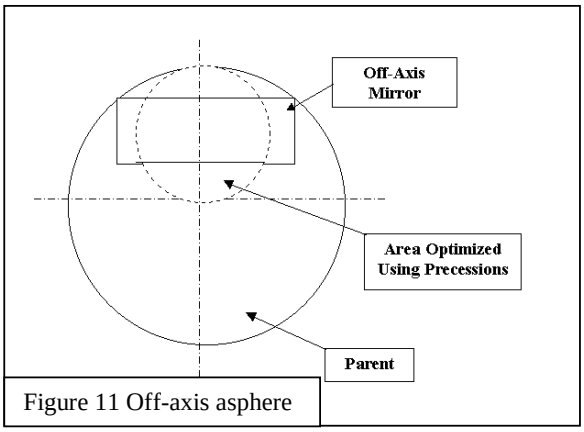

Figure 11 Off-axis asphere

We have assumed that the base asphere would be pre-machined using a precision diamond grinding machine, and that *Precessions* polishing would remove a form error of ~9 microns p-to-v. This was simulated by a parabolic error term. We used experimental tool influence function data, that was scaled to a larger size commensurate with the dimension of the mirror. The *Precessions* optimiser was then run on the target and error profiles in the region shown in Figure 11, and a spiral tool-path computed. The result in terms of material removal was calculated and used to predict the final form of the surface. This is shown in Figure 12. Over the area to be used, the result is essentially perfect.

In practice, to create the 3-dimensional form of the off-axis segment, the work-piece would be rastered rather than spiralled. However, the effect of the tool on the aspheric form would be essentially the same, and therefore the result of the simulation presented here may indicate the feasibility of *Precessions* polishing to address aspheres of this type. It remains to extend the *Precessions* optimisation code to full 3-D capability, as the machine and its CNC control system can already support the rastering function.

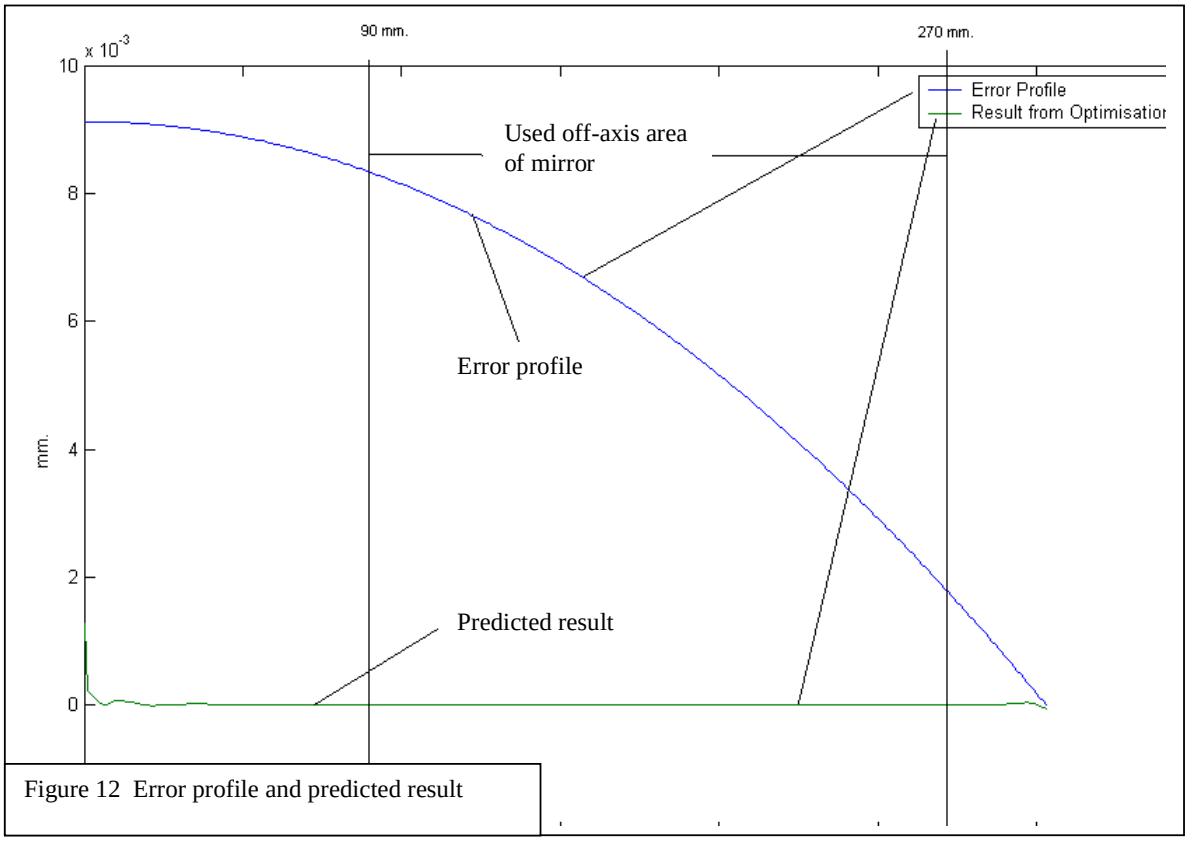

Figure 12 Error profile and predicted result

9. Conclusions

We have demonstrated the ability of the membrane tooling to remove a 7.5 micron deep layer from an aspheric surface, with a uniformity exceeding 90%. The asphere in question was, by astronomical standards, extreme in its ratio of 125 microns aspheric departure from sphere osculating at the vertex, over 40mm of diameter). This showed that the tooling very effectively accommodated the change in surface curvature across the work-piece surface, and that overall process uniformity was excellent. This result has been reinforced by running the *Precession* optimisation code in simulation-mode and demonstrating the ability to correct form on a difficult asphere of interest to the space-astronomy community.

We have then reported on the first experiment to conduct iterative cycles of fine form control. A nominally flat surface with about 0.1 microns of error was figured into a Schmidt-like profile removing some 0.6 microns of material in total. 80nm peak-to-valley form error was achieved in three runs. We have highlighted the difficulty of very short dwell-times in fine form control, and outlined our strategy to overcome this limitation.

Using simple geometric arguments, we have shown that the *Precessions* process is scalable to larger work-piece and tool sizes. In this respect, work-in-progress is showing that the process is a strong candidate for polishing and figuring of segments for extremely large telescopes, given extension of the optimisation code to handle non-axially-symmetric forms. Combining the results on form-preservation of a highly aspheric form, and fine form-control on a mild aspheric, gives us confidence that *Precessions* polishing (with further development) will satisfy a wide range of astronomical requirements. These include instrumentation optics, correction of quilting in honeycomb mirror substrates, and ELT segment manufacture.

Excellent texture from the *Precessions* process has been demonstrated on a range of materials. The formation of ripple of spatial frequencies equivalent to the tool spot-size and the step-size between tool-passes, has been considered in some detail. From the preliminary results, the ripple specification of the Euro50 primary segments should be achievable with *Precessions* polishing. We have modelled the diffraction effect of ripple on point-spread function and considered different possible tool-paths. Given the ability of the CNC polishing hardware to execute almost any tool-path for which it is programmed, this gives an invaluable method in developing and optimising polishing strategies.

Finally, edge roll-off does not appear to be a major problem with *Precessions* polishing, as shown by a preliminary result obtained with no specific process-optimisation for edges. With development of the process, edges should be simple to control.

Acknowledgements

We wish to thank the UK Particle Physics and Astronomy Research Council and the Defence Science and Technology Laboratory of the Ministry of Defence, for financial support of the work at UCL. We also acknowledge the contribution of Loh Optikmaschinen in collaborative process development using the IRP200 machine sited at their premises.

References

1. "From VLT to OWL: science and technology of ESO's 100m telescope concept", R. Gilmozzi, proc. SPIE conference 'Future Giant Telescopes', Hawaii, vol. 4840, 2002, in print

2. "Progress on the Californian Extremely Large Telescope (CELT)", J.E. Nelson, proc. SPIE conference 'Future Giant Telescopes', Hawaii, vol. 4840, 2002, in print

3. "Giant Segmented Mirror Telescope: a point design based on Science Drivers", S.E. Strom, L.M. Stepp, B. Gregory, proc. SPIE conference 'Future Giant Telescopes', Hawaii, vol. 4840, 2002, in print

4. "Euro50 extremely large telescope", T. Andersen, A Ardeberg, A. Goncharov, M. Owner-Petersen, H. Riewaldt, R. Snell, J. Becquers, D. Walker, proc. SPIE conference 'Future Giant Telescopes', Hawaii, vol. 4840, 2002, in print

5. "The Primary and Secondary Mirrors for the Proposed Euro50 Telescope", D. Walker et.al., a study commissioned by Instituto de Astrofisica de Canarias on behalf of the Euro50 Project

6. "Lessons learnt in the optical design of the Next Generation Space Telescope", J.B. Hadaway, M. Wilson, D. Redding, B. Woodruff, proc. SPIE conference 'Space Telecopes and Instruments V', Hawaii, vol. 3356, 1998, pp114-121

7. "Practical design and performance of the stressed-lap polishing tool", C.West et.al., App Opt., 33(34) 8094-8100, 1994

8. "Fabrication and measurement quality of the MMT primary mirror", H.M. Martin, et.al., Proc. SPIE 3352 194-204, 1998

9 "Novel CNC polishing process for control of form and texture on aspheric surfaces", D.D. Walker, A.T.H. Beaucamp, D. Brooks, R. Freeman, A. King, G. McCavana, R. Morton, D. Riley, J. Simms, proc. 47th An. Mtg SPIE, Seattle, in print

10. "The first aspheric form and texture results from a production machine embodying the Precession process": D.D. Walker, D. Brooks , R. Freeman, A. King , G.McCavana, R. Morton, D. Riley, J. Simms, proc. Proc. SPIE 46th Annual Meeting, the International Symposium on Optical Science and Technology, San Diego, 2001, vol. 4451, 2001, pp267-276

11. "The Zeeko/UCL Process for Polishing Large Lenses and Prisms" D.D. Walker, R. Freeman, G. McCavana, R. Morton, D. Riley, J. Simms, D. Brooks, A. King, proc. Large Lenses and Mirrors conference, UCL, March 2001, pub. SPIE, pp 106-111

12. "A Novel Automated Process for Aspheric Surfaces" R,G. Bingham, D.D. Walker, D-H. Kim, D. Brooks, R. Freeman, D. Riley , Proc. SPIE 45th Annual Meeting, the International Symposium on Optical Science and Technology, 2000, Vol. 4093 'Current Developments in Lens Optical Design and Engineering'; pp445-448

13. Born and Wolf 6th edition 1980 section 9.1

14. Introduction to Surface Roughness and Scattering, by Jean M. Bennett and Lars Mattsson, Opt. Soc. of America 1989